Model for the Path Loss of In-room Reverberant Channels

Steinböck, Gerhard; Pedersen, Troels; Fleury, Bernard Henri; Wang, Wei; Jost, Thomas; Raulefs, Ronald

Published in:
I E E E V T S Vehicular Technology Conference. Proceedings

DOI (link to publication from Publisher):
10.1109/VETECS.2011.5956709

Publication date:
2011

Document Version
Early version, also known as pre-print

Model for the Path Loss of In-room Reverberant Channels

Gerhard Steinböck[1)], Troels Pedersen[1)], Bernard H. Fleury[1)], Wei Wang[2)], Thomas Jost[2)] and Ronald Raulefs[2)]

[1)]Dept. of Electronic Systems,
Section Navigation and Communications,
Aalborg University
Fredrik Bajers Vej 7, DK-9220 Aalborg East, Denmark
Email: {gs, troels, bfl}@es.aau.dk

[2)]Institute of Communications and Navigation,
German Aerospace Center (DLR)
Oberpfaffenhofen, 82234 Wessling, Germany
Email: {Wei.Wang, Thomas.Jost, Ronald.Raulefs}@DLR.de

***Abstract*—A general path loss model for in-room radio channels is proposed. The model is based on experimental observations of the behavior of the delay-power spectrum in closed rooms. In such a room, the early part of the spectrum observed at different positions typically consists of a dominant component (peak) that vanishes as the transmitter-receiver distance increases; the late part decays versus distance according to the same exponential law in delay regardless of the distance. These observations motivate the proposed model of the delay-power spectrum with an early dominant component and a reverberant component. The dominant component is modeled as a Dirac delta function weighted with a factor decaying according to an inverse distance power law (d^{-n}). The reverberant component is an exponentially decaying function versus delay with distance-dependent onset. Its power decays exponentially with distance. The proposed model allows for the prediction of path loss, mean delay, and rms delay spread versus distance. We use measurements to validate the model. We observe good agreement of the model prediction for mean delay and rms delay spread.**

I. Introduction

The field of indoor radio-localization has recently attracted significant interest. One approach for solving the localization problem is to rely on the measured power of the received signal [1] and to use a path loss model to infer the corresponding length of a radio link. Knowledge of the received power is often used for localization in already deployed systems (e.g. WiFi) where received signal strength is readily available or with cheap low power devices in sensor networks. Even when deploying localization techniques with higher accuracy, path loss models are used to predict the signal-to-noise ratio and the probability of connectivity [2], which are both important criteria for system analysis.

Indoor path loss models, relating the received power to the transmitter-receiver distance, have been a valuable instrument to the communication engineer [3]. A vast amount of such models have been proposed for various propagation scenarios and environments and have been validated for diverse purposes in wireless communications. The primary concern so far has been to predict the power loss with respect to distance. These models consider indoor scenarios in which path loss is caused by transmission across multiple walls and floors, and multi-path fading [4], [5]. Thus, they cover a whole building. Only few models are available in the literature that characterize propagation in a single room [6].

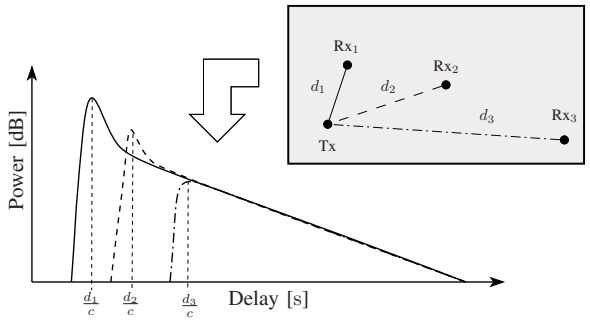

Fig. 1. Typical behavior of the bandlimited delay-power spectrum experimentally observed in an in-room environment at three different transmitter-receiver distances (schematically presented by the grey box).

In this contribution we propose an in-room path loss model based on experimental observations of the behavior of the delay-power spectrum [7], [8] and on analogies to models used in room acoustics [9] and electromagnetic fields in cavities [10]. In our model the delay-power spectrum consists of a dominant and a reverberant component. The model allows for the prediction of the path loss, the mean delay and the rms delay spread versus transmitter-receiver distance. The proposed model is validated with a new set of measurement data.

II. Delay Power Spectrum Model

We consider an in-room scenario as illustrated in Fig. 1. The delay-power spectrum is observed at different transmitter and receiver locations. A system bandwidth high enough to observe frequency fading (delay dispersion), but to low to separate single propagation paths in the environment is considered. The regarded carrier frequencies are high enough, such that the smallest dimension of the room is large compared to the wavelength λ. The delay-power spectrum is the expectation of the squared magnitude of the impulse response $h(\tau, d)$:

$$G(\tau, d) = \mathrm{E}[|h(\tau, d)|^2]. \tag{1}$$

Here τ is the delay and d is the transmitter-receiver distance. In [8] it is observed that the delay-power spectrum in such

TABLE I
PARAMETERS OF THE PROPOSED MODEL.

Parameter	Meaning
G_0	Path gain at reference distance d_0.
d_0	Reference distance, typically 1 m.
n	Path gain decay exponent of the dominant component.
q	Ratio $G_{\mathrm{rev}}(d_0)/G_{\mathrm{dom}}(d_0)$.
T	Reverberation time of the reverberant component.

an in-room scenario exhibits the typical behavior depicted in Fig. 1. The tail of the delay-power spectrum exhibits the same constant exponential decay regardless of the transmitter-receiver distance. The early part is strong at short distance and gradually vanishes as this distance increases.

Based on these observations, we model the delay-power spectrum as a dominant component plus a reverberant component:

$$\begin{aligned} G(\tau, d) &= \mathrm{E}[|h_{\mathrm{dom}}(\tau, d)|^2] + \mathrm{E}[|h_{\mathrm{rev}}(\tau, d)|^2] \\ &= G_{\mathrm{dom}}(\tau, d) + G_{\mathrm{rev}}(\tau, d). \end{aligned} \tag{2}$$

Subscript dom indicates the dominant component and subscript rev denotes the reverberant component. The dominant component represents the early part of the delay-power spectrum consisting of a directly propagating component and possible first-order reflections from the floor, ceiling and walls. The reverberant component represents the multitude of higher order reflections in the room which yield the diffuse tail of the delay-power spectrum.

We model the delay-power spectrum of the dominant component as

$$G_{\mathrm{dom}}(\tau, d) = G_0 \left(\tfrac{d_0}{d}\right)^n \delta\left(\tau - \tfrac{d}{c}\right), \tag{3}$$

where n is the power decay exponent, $\delta(\cdot)$ is the Dirac delta function, c the speed of light, and $G_0 > 0$ is the gain at the reference distance d_0.

We model the reverberant delay-power spectrum as an exponentially decaying function with onset determined by the transmitter-receiver distance:

$$G_{\mathrm{rev}}(\tau, d) = \begin{cases} G_{0,\mathrm{rev}}\, e^{-\frac{\tau}{T}}, & \tau > \frac{d}{c} \\ 0, & \text{otherwise} \end{cases} \tag{4}$$

where $G_{0,\mathrm{rev}}$ is the reference gain of the reverberant component. In analogy to acoustics [8], [9] we call T the reverberation time.

We remark that the models in [7] and [8] are based on the room acoustic theory. They both neglect the transmitter-receiver distance. In [7] the delay-power spectrum of the reverberant component, i.e. corresponding to (4), is non-exponential. It has maximum power one and constant onset at delay zero. In [8] the model only accounts for the exponentially decaying delay-power spectrum of the reverberant component in (2).

III. PREDICTIONS OF THE DELAY POWER SPECTRUM MODEL

Based on the model (2) we now derive expressions for the path gain, mean delay, and rms delay spread as a function of the transmitter-receiver distance.

A. Path gain

The path gain at distance d is

$$\begin{aligned} G(d) &= \int G(\tau, d)\mathrm{d}\tau \\ &= \underbrace{G_0 \left(\tfrac{d_0}{d}\right)^n}_{G_{\mathrm{dom}}(d)} + \underbrace{G_{0,\mathrm{rev}}\, T\, e^{\frac{-d}{c\,T}}}_{G_{\mathrm{rev}}(d)}. \end{aligned} \tag{5}$$

The component $G_{\mathrm{dom}}(d)$ decays with d^{-n}, while $G_{\mathrm{rev}}(d)$ decays exponentially. Denoting by q the ratio of reverberant to dominant gain at reference distance d_0:

$$q = \frac{G_{\mathrm{rev}}(d_0)}{G_{\mathrm{dom}}(d_0)} = \frac{G_{0,\mathrm{rev}}}{G_0}\, T\, e^{\frac{-d_0}{c\,T}}, \tag{6}$$

the path gain can be recast as

$$G(d) = G_0 \left(\tfrac{d_0}{d}\right)^n + G_0\, q\, e^{\frac{d_0 - d}{c\,T}}. \tag{7}$$

Examples of $G(d)$ are graphed in Fig. 2a. At small distances $G_{\mathrm{dom}}(d)$ dominates and the path gain decays as d^{-n}. Beyond a certain distance, the contribution of the reverberant component $G_{\mathrm{rev}}(d)$ in $G(d)$ leads to a deviation from $G_{\mathrm{dom}}(d)$. This effect occurs over a certain distance interval, denoted as the reverberation region $D_{\mathrm{rev}} = \{d : G_{\mathrm{rev}}(d) \geq G_{\mathrm{dom}}(d)\}$. At larger distances $G_{\mathrm{rev}}(d)$ vanishes and $G(d)$ approaches $G_{\mathrm{dom}}(d)$ again.

We remark that the path loss is defined as the inverse of the path gain: $L(d) = G(d)^{-1}$. For notational convenience we consider only path gain in the sequel.

B. Mean Delay and Root Mean Squared Delay Spread

The mean delay at distance d as is derived from (2) as

$$\mu_\tau(d) = \frac{1}{G(d)} \int \tau\, G(\tau, d)\mathrm{d}\tau \tag{8}$$

$$= \tfrac{d}{c} + T \frac{1}{1 + \left(\tfrac{d_0}{d}\right)^n \tfrac{1}{q}\, e^{\frac{d - d_0}{c\,T}}}. \tag{9}$$

In (9) the first term is the delay of a directly propagating component and the second term results from the reverberant component. Fig. 2b depicts the mean delay versus distance with the settings specified in the legend of the figures. The mean delay increases with distance. For distances in the reverberation region, the curves approximately follow the straight line $\frac{d}{c} + T$. It can be seen from (9) that $\lim_{d \to 0} \mu_\tau(d) = 0$ and that $\mu_\tau(d)$ has the asymptote $\frac{d}{c}$ for $d \to \infty$. Note that the range of distance considered in the plot of Fig. 2b is to small to observe the convergence of $\mu_\tau(d)$ towards its asymptote.

Similarly, (2) enables computation of the rms delay spread: $\sigma_\tau(d)$:

$$\sigma_\tau^2(d) = \frac{1}{G(d)} \int \tau^2\, G(\tau, d)\mathrm{d}\tau - \left(\mu_\tau(d)\right)^2. \tag{10}$$

Insertion of (7) and (9) into (10) leads to

$$\sigma_\tau^2(d) = \frac{T^2}{1 + \left(\tfrac{d_0}{d}\right)^n \tfrac{1}{q}\, e^{\frac{d - d_0}{c\,T}}} \left(2 - \frac{1}{1 + \left(\tfrac{d_0}{d}\right)^n \tfrac{1}{q}\, e^{\frac{d - d_0}{c\,T}}}\right). \tag{11}$$

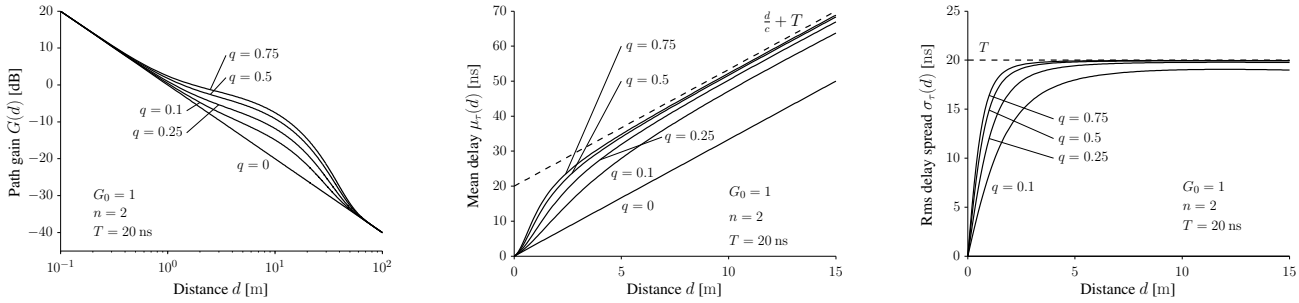

(a) (b) (c)

Fig. 2. Path gain (a), mean delay (b) and rms delay spread (c) versus distance predicted by the proposed model for $d_0 = 1$ m.

Fig. 2c depicts the rms delay spread versus distance. Notice, $\sigma_\tau(d)$ in (11) has the following limits

$$\lim_{d\to 0} \sigma_\tau(d) = \lim_{d\to\infty} \sigma_\tau(d) = 0. \tag{12}$$

Here again, the range of the distance considered in Fig. 2c is to small to observe the convergence of $\sigma_\tau(d)$ towards 0 as $d \to \infty$. For distances in the reverberation region $\sigma_\tau(d)$ approaches the reverberation time T. Indeed it can be shown that

$$T = \sup_{d,n,q} \{\sigma_\tau(d) : d \geq 0, n \geq 0, q \geq 0\}, \tag{13}$$

i.e. the rms delay spread is upper bounded by T for any distance.

IV. Measurement Data

We validate the proposed model by means of measurement data from a campaign conducted at DLR in Oberpfaffenhofen, Germany. The investigated room is sketched in Fig. 3. A panograph of it is depicted in Fig. 4. The environment was static and no one was in the room while the measurements were taken.

The dimensions of the room are $5.1 \times 5.25 \times 2.78\,\mathrm{m}^3$. The three inner walls are made of plaster boards. As visible in the panograph, the outer "wall" consists mainly of four windows (W1–W4) and two pillars made of concrete. The frames of the windows are metallic and the glass is metal coated. The height of the transmit and receive antenna was $1.26\,\mathrm{m}$ and $1.1\,\mathrm{m}$, respectively.

The measurement data were collected using the Rusk-DLR channel sounder [11] operating at $5.2\,\mathrm{GHz}$. The settings of the sounder are summarized in Table II. The transmit antenna [12] was omni-directional with 3 dBi gain. A uniform circular array of eight monopoles with diameter $75.18\,\mathrm{mm}$ was used at the receiver. The transmitter and receiver were synchronized to a common clock via cables throughout the measurements.

The equipment used a multiplexer to sequentially sound the eight channels between the port of the transmit antenna and the ports of the eight elements of the receive array. One measurement cycle, in which all eight channel frequency responses were measured, was completed in $204.8\,\mu\mathrm{s}$. The sounder was operating in "burst" mode. In each burst 20 consecutive measurement cycles were performed. One burst lasted $20 \cdot 204.8\,\mu\mathrm{s} = 4096\,\mu\mathrm{s}$. Between each burst, the

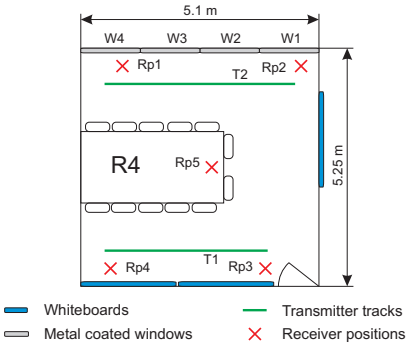

Fig. 3. Schematic of the investigated room.

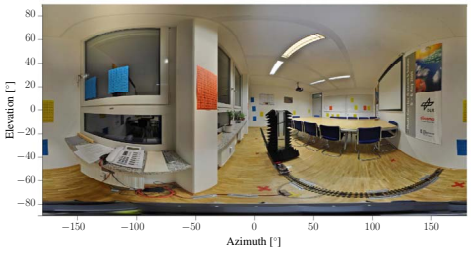

Fig. 4. Panograph (spherical panoramic photo) of the investigated room seen from Rp1 using an equi-rectangular projection.

sounder paused for data storage; the burst repetition time was $131.072\,\mathrm{ms}$.

The receive antenna array was placed at five fixed locations labeled as Rp1 to Rp5 respectively in Fig. 3. The transmit antenna was mounted on a model train which moved on two tracks labeled as T1 and T2. Frequency responses were measured for each receiver position while the transmitter moved along the two tracks with a constant speed of approximately $0.05\,\mathrm{m/s}$. During one measurement burst the transmitter moved $204.8\,\mu\mathrm{m} = 0.0035\lambda$. Over this distance the channel response can be considered constant. Between two consecutive bursts, the transmitter moved $6.55\,\mathrm{mm} \approx \lambda/8.8$.

The positions Rp1-Rp5 and the trajectory along the track were measured with a tachymeter. The odometer of the model train was connected to the channel sounder to record the measurement locations.

V. Results

We compute the received power at all receiver and transmitter positions. Notice that one measurement burst corresponds uniquely to one pair of transmitter and receiver positions. Let us consider one specific burst. The frequency responses of each of the eight channels measured during the burst are averaged.

TABLE II
SETTINGS OF THE CHANNEL SOUNDER.

Parameter	Value
Carrier frequency f_c	5.2 GHz
Bandwidth B	120 MHz
Number of sub-carriers N_c	1536
Carrier separation Δf	78.125 kHz
Signal duration	12.8 µs
Cycle duration	204.8 µs
Cycles per burst	20
Burst duration	4096 µs
Burst repetition time	131.072 ms
Transmit power	0 dBm

TABLE III
PARAMETER ESTIMATES FOR THE STANDARD AND PROPOSED MODELS.

Model	$\widehat{G}_0$	$\widehat{n}$	$\widehat{q}$	$\widehat{T}$ [ns]
Standard	$1.11 \cdot 10^{-5}$	1.14	—	—
Proposed $\widehat{T} = 18.73$ ns	$6.42 \cdot 10^{-6}$	2.26	0.56	18.73
Proposed $\widehat{T} = 16.02$ ns	$5.79 \cdot 10^{-6}$	2.39	0.71	16.02

The averaged responses are then squared and integrated to obtain the power values of the eight channels. Averaging these values yields the power measured in the burst. Fig. 5 reports the scatter plot of power values computed for all bursts versus transmitter-receiver distance. Since the noise-floor is below -70 dBm in all measurements, we disregard the noise.

We compute the mean delay estimate $\widehat{\mu}_\tau$ and rms delay spread estimates $\widehat{\sigma}_\tau$ for each burst. We multiply the averaged frequency responses of the eight channels obtained for a given burst (see above) with a Hann window. Taking the inverse Fourier transform of the filtered frequency responses yields estimates of the impulse responses of the eight channels. The mean delay and delay spread estimates for the burst are obtained by inserting the squared average of the eight impulse responses in (8) and (10), respectively. These estimates computed for all bursts are reported versus transmitter-receiver distance in Fig. 6. These values are in accordance with values reported in [5] for office environments.

We use the model assumption (4) on the behavior of the tail of the delay-power spectrum versus τ to estimate T from experimental delay-power spectra. More specifically, an estimate of T is obtained from a linear least squares estimate of the slope of the late part of the experimental log power spectra. As can be seen in Fig. 7 the underlying model assumption (4) holds true for the experimental delay-power spectra. Considering the restriction of the log spectra obtained for any transmitter and receiver positions in the delay range $40\text{ ns} \leq \tau \leq 150\text{ ns}$, the linear least squares estimator yields $\widehat{T} = 18.73$ ns.

We test the behavior of the mean delay ($\mu_\tau \to \frac{d}{c} + T$, see Fig. 2b) and the rms delay spread ($\sigma_\tau \approx T$, see Fig. 2c) predicted by the model when d ranges in the reverberation region. The scatter plot of estimates of the rms delay spread in Fig. 6 shows a constant behavior for distances larger than 3 m. Therefore, we estimate T by taking the average of these estimates for $d > 3$ m. This yields $\widehat{T} = 16.02$ ns. Similarly we estimate T from the scatter plot of estimates of the mean delay versus distance. For each estimate, say $\widehat{\mu}_\tau(d)$, the difference $\widehat{\mu}_\tau(d) - \frac{d}{c}$ is computed for $d > 3$ m. The estimate $\widehat{T}$ is the

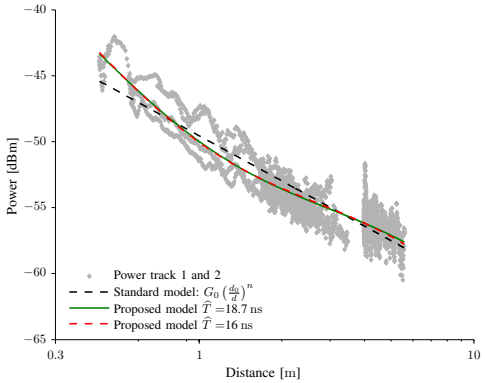

Fig. 5. Estimated received power versus distance with the predictions computed using the standard and the proposed path gain models.

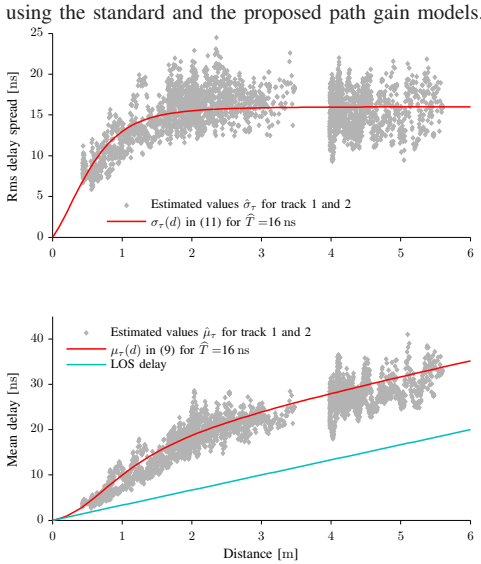

Fig. 6. Scatter plots of estimates of the rms delay spread and the mean delay versus distance. The solid lines depict the predicted rms delay spread and mean delay obtained with the proposed model. For reference we also plot the line corresponding to $\frac{d}{c}$.

average of these differences. Doing so yields $\widehat{T} = 13.07$ ns. The theoretical results for μ_τ and σ_τ in Fig. 2b and Fig. 2c, respectively, show that for some model parameter settings, the bound $\sigma_\tau \approx T$ and specifically the asymptote of the mean delay $\mu_\tau \to \frac{d}{c} + T$ are not reached. Thus we proceed with the analysis by considering the two close estimates $\widehat{T} = 18.73$ ns and $\widehat{T} = 16.02$ ns.

We estimate the parameters of both the standard path loss model ($G(d) = G_0\left(\frac{d_0}{d}\right)^n$) and the proposed model from the estimated power values reported in Fig. 5. More specifically, the estimates are computed by considering the log-power domain. For the standard path loss model a linear least squares estimation is performed. We use the Matlab curve fitting toolbox [13], which provides a non-linear least squares estimator, to fit the proposed path gain model (7). This toolbox returns estimates of the parameters G_0, n and q with the estimate $\widehat{T}$ provided as input.

The estimates of the parameters of the models are reported in Table III and the path gains versus distance computed from the models with these parameter settings are shown in Fig. 5. The path gain predictions of the standard and proposed models (for the two sets of parameter estimates) almost overlap.

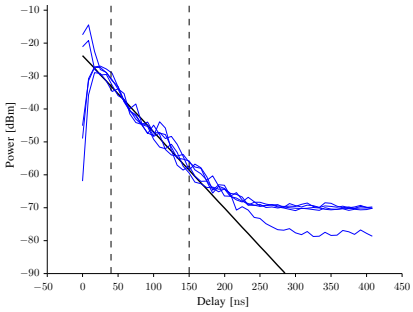

Fig. 7. Spatially averaged delay-power profiles obtained for the receiver positions Rp1 to Rp5 when the transmitter was at the start position on track T1. The straight line depicts an exponentially decaying function with decay factor $\widehat{T} = 18.73\,\mathrm{ns}$. The dashed lines indicate the range $40\,\mathrm{ns} \leq \tau \leq 150\,\mathrm{ns}$ used for the estimation of $\widehat{T}$.

VI. Discussion

The estimate $\widehat{n} = 1.14$ of the path loss exponent of the standard path gain model is in the range of published values obtained from in-room measurement data [6] and references therein. Traditionally, exponent values lower than 2 are attributed to wave guiding effects. However, the dimensions of the room do not advocate this interpretation. A reverberation phenomenon in the room provides a more plausible explanation to the observed low exponent.

The estimates of the mean delay $\widehat{\mu}_\tau(d)$ and rms delay spread $\widehat{\sigma}_\tau(d)$ shown in Fig. 6 are in accordance with the model prediction obtained with $\widehat{T} = 16.02\,\mathrm{ns}$. The predicted transition of the mean delay and the rms delay spread from zero at $d = 0$ to respectively $\frac{d}{c} + T$ and T for d ranging in the reverberation region is well observed.

The parameter estimates of the model computed from the two estimated reverberation times slightly differ (see Table III). However, the path gains predicted by the two model estimates fall on top of each other as shown in Fig. 7.

The estimate $\widehat{T} = 18.73\mathrm{ns}$ obtained directly from the delay-power spectra deviates by only 14.5 % from $\widehat{T} = 16.02\,\mathrm{ns}$ obtained from (13). These observations support the hypothesis that the reverberant component impacts significantly the received power, mean delay, and rms delay spread.

The estimated values for q, which characterize the ratio between the power of the dominant and reverberant components, is 0.56 and 0.71 respectively. Thus, the reverberant component plays an important role in the description of the path gain. The estimates $\widehat{n} = 2.26$ and 2.39 of the path gain decay exponent of the dominant component are close to the exponent of free-space propagation.

The estimated reverberation times are close to typical rms delay spreads observed in office environments [5]. This suggests that these rms delay spreads might have been measured in the reverberation region and are thus dominated by the reverberation term. This interpretation is further supported by the fact that the reverberation region starts as close a distance as $1.2\,\mathrm{m}$ in the considered scenario.

VII. Conclusions

A model of the delay-power spectrum of an in-room reverberant channel has been proposed. The model includes a dominant and a reverberant component. The dominant component follows an inverse distance power law (d^{-n}). The reverberant component decays exponentially versus delay and exhibits a distance dependent onset. As a result, its power decays exponentially with distance. The proposed model allows for the prediction of path gain, mean delay and rms delay spread. The model was validated using measurement data and compared to the standard path loss model. The predictions of mean delay and rms delay spread agree well with the estimates obtained from the measurement data. In the investigated environment the ratio of the gain of the reverberant component to the gain of the dominant component is 0.56. Hence, the reverberant component is prominent in this environment. The estimated path gain exponent of the dominant component in the proposed model is close to the free-space path gain exponent. Due to its inability to separate the dominant component from the reverberant component the standard path gain model yields a path gain exponent close to unity. This model merely provides a fit of the path gain that blends the contributions from the dominant and reverberant component.

Acknowledgment

This work was supported by the ICT-216715 FP7 Network of Excellence in Wireless COMmunication (NewCom++) and by the project ICT-248894 Wireless Hybrid Enhanced Mobile Radio Estimators – Phase 2 (WHERE2).

References

[1] H. Liu, H. Darabi, P. Banerjee, and J. Liu, "Survey of Wireless Indoor Positioning Techniques and Systems," *IEEE Trans. Syst., Man, Cybern. C*, vol. 37, no. 6, pp. 1067–1080, Nov. 2007.

[2] D. Dardari, A. Conti, C. Buratti, and R. Verdone, "Mathematical Evaluation of Environmental Monitoring Estimation Error through Energy-Efficient Wireless Sensor Networks," *IEEE Trans. Mobile Comput.*, vol. 6, no. 7, pp. 790–802, July 2007.

[3] R. Vaughan and J. B. Andersen, *Channels, Propagation and Antennas for Mobile Communications*. Institution of Engineering and Technology, 2003.

[4] J. Keenan and A. Motley, "Radio coverage in buildings," in *Br. Telecom Technol. J.*, vol. 8, no. 1, Jan. 1990, pp. 19–24.

[5] E. Damosso, Ed., *Digital mobile radio towards future generation systems: COST 231 Final Report*. Bruxelles, Belgium: European Commission, 1999.

[6] D. Xu, J. Zhang, X. Gao, P. Zhang, and Y. Wu, "Indoor Office Propagation Measurements and Path Loss Models at 5.25 GHz," *IEEE Veh. Technol. Conf. (VTC)*, pp. 844–848, Oct. 2007.

[7] C. Holloway, M. Cotton, and P. McKenna, "A model for predicting the power delay profile characteristics inside a room," *IEEE Trans. Veh. Technol.*, vol. 48, no. 4, pp. 1110–1120, 1999.

[8] J. B. Andersen, J. Ø. Nielsen, G. F. Pedersen, G. Bauch, and J. M. Herdin, "Room electromagnetics," *IEEE Antennas Propag. Mag.*, vol. 49, no. 2, pp. 27–33, 2007.

[9] H. Kuttruff, *Room Acoustics*, 4th ed. London: Taylor & Francis, 2000.

[10] D. A. Hill, *Electromagnetic Fields in Cavities: Deterministic and Statistical Theories*, ser. IEEE Press Series on Electromagnetic Wave Theory. Piscataway, NJ: Wiley/IEEE Press, 2009.

[11] J. Stephan, Y. Lostanlen, J. Keignart, W. Wang, D. Slock, and F. Kaltenberger, "Measurements of location-dependent channel features," ICT-217033 WHERE, Del. 4.1, Oct. 2008, http://www.ict-where.eu/.

[12] Huber+Suhner, "Datasheet for Sencity Antenna For In-Carriage Wireless Communication, Type: SOA 5600/360/3/20/V_1," Document No. 01.02.1358, May 2007.

[13] Mathworks, "Matlab Curve Fitting Toolbox, Version 1.2.2 (r2008b)," 2008.